Abstract of the report and proposal to extend

Search for new physics in experiments with the Fermilab high-intensity muon beams (02-2-1124-2015/2017)

Проект: Поиск новой физики в экспериментах на интенсивных пучках мюонов Фермилаб

1. INTRODUCTION

It is expected that in the next decade discoveries at colliders will help illuminate more fully the particle content of whatever New Physics (NP) model best describes Mother Nature. To get a more thorough understanding of the underlying dynamics responsible for the NP requires a plethora of measurements the colliders can't do. These include determining the parameters of the PMNS matrix, probing the parameters of the CKM matrix, searching for evidence of mixing in the charged lepton sector (charged lepton flavor violation – CLFV), searches for baryon number violating processes, and direct searches for dark matter candidates.

The muon anomalous magnetic moment a_μ is a low-energy observable, which can be both measured and computed to high precision. The comparison between experiment and the SM therefore provides a sensitive search for NP. At present, both measurement and theory have sub-part-per-million (ppm) uncertainties, and the "g-2 test" is being used to constrain SM extensions. The difference between experiment and theory, Δa_μ(Expt- SM) = (274 ± 76) × 10^{-11} (3,6 σ), is a highly cited result and a possible harbinger of new TeV-scale physics. Potential explanations of the deviation include: supersymmetry, lepton substructure, dark matter loop etc., all well motivated by theory and consistent with other experimental constraints. Fermilab Proposal-989[1] has a plan to reduce the experimental uncertainty by a factor of 4 or more. This reduction will lead to a more definitive result - $\Delta a_\mu > 5\sigma$ "discovery-level" deviation from the SM - if the central value remains unchanged. A precise g-2 test, no matter where the final value lands, will sharply discriminate among models and will enter as one of the central observables in a global analysis of any SM extensions.

The recently proposed Mu2e experiment at Fermilab [2] is a dedicated search for the CLFV process $\mu^- N \rightarrow e^- N$, which is the coherent conversion of a muon into an electron in the vicinity of a nucleus. Strictly speaking this process is forbidden in the SM. Once neutrinos masses are included, the process is allowed but effectively still absent since the rate is proportional to $\left(\Delta m_{ij}^2 / M_w^2\right)^2$, where Δm_{ij}^2 is the mass difference squared between *ith* and *jth* neutrino mass eigenstates, and M_W is the mass of the W-boson. For example, the predicted rates for the $\mu^- N \rightarrow e^- N$ and $\mu^+ \rightarrow e^+\gamma$ CLFV processes are less than 10^{-50} each [3]. This makes these processes a very theoretically clean place to search for NP effects. In many NP models that include a description of neutrino mass, the rates for these processes are enormously enhanced so that they occur at a level to which next generation experiments will have sensitivity. An ambitious experiment to study this physics was proposed for the AGS at Brookhaven. Called the Muon to Electron COnversion (MECO) experiment, it was based on a muon beam line concept that was first proposed for the MELC experiment [4] at the Russian Institute for Nuclear Research (INR) a few years earlier.

There are a variety of CLFV experiments with sensitivities approaching theoretically interesting regions. These include CLFV tau lepton, muon, kaon, and b-meson decays. Among these the $\mu^- N \rightarrow e^- N$ process has sensitivity to the broadest array of NP models. Like the $\mu^+ \rightarrow e^+\gamma$, $\mu^+ \rightarrow e^+e^-e^+$, or $\tau^+ \rightarrow \mu^+\gamma$ processes, $\mu^- N \rightarrow e^- N$ is sensitive to NP contributions via loops, such as those expected in Supersymmetry via slepton mixing, induced in seasaw models of Heavy Neutrinos, and present in two Higgs doublet models. In addition, the $\mu^- N \rightarrow e^- N$ process is also sensitive to NP contributions via contact interactions, such as those expected in Compositeness, Leptoquark, and GUT models with additional gauge bosons and/or anomalous couplings [3]. The

above models predict rates as large as 10^{-15} in regions of phase space that overlap with LHC discovery sensitivities. For Phase-I the target discovery sensitivity on the rate of the $\mu^- N \rightarrow e^- N$ process, $R_{\mu e}$,

$$R_{\mu e} = \frac{\mu^- + A(Z,N) \rightarrow e^- + A(Z,N)}{\mu^- + A(Z,N) \rightarrow \nu_\mu + A(Z-1,N)}$$

is less than 10^{-16} and offers the Mu2e experiment great discovery potential over a wide array of NP models and enables it to probe mass scales as large at 10^4 TeV, well beyond what will be explored at the LHC. The ratio of rates among various CLFV processes is model dependent and can differ by orders of magnitude. Measuring the rates of several CLFV processes will be important in elucidating the details of the underlying NP model.

A muon-to-electron conversion experiment at Fermilab could provide an advance in experimental sensitivity of four orders of magnitude. The experiment could go forward in the next decade with a modest evolution of the Fermilab accelerator complex. Such an experiment could be the first step in a world-leading muon-decay program eventually driven by a next-generation high-intensity proton source. Development of a muon-to-electron conversion experiment should be strongly encouraged in all budget scenarios considered by the Fermilab.

1.0 Mu2e-II is the next perspective stage of experiment

Proton Improvement Plan-II (PIP-II) is the centerpiece of Fermilab's plan for upgrading the accelerator complex to establish the leading facility in the world for particle physics research based on intense proton beams. PIP-II has been developed to provide 1.6 MW of proton beam power at the start of operations of the Long Baseline Neutrino Facility (LBNF), while simultaneously providing a platform for eventual extension of LBNF beam power to >2 MW and enabling future initiatives in rare processes research based on high duty factor/higher beam power operations. PIP-II is based on the construction of a new 800 MeV superconducting linac, augmented by improvements to the existing Booster, Recycler, and Main Injector complex. To achieve another factor of ten improvement in sensitivity, Mu2e-II will require about 100-kW. The linac will have the possibility of being further upgraded to proton energies as high as 3-GeV. The present Mu2e design is optimized for 8-kW of protons at 8 GeV.

1.1 Muon g-2 and Mu2e works together

The muon g-2, together with searches for charged lepton flavor violation, electric dipole moments, and rare decays, provides such a complementary tool to probe the high energy frontier.

The complementarity between these different measurements can be obviously seen. G-2 corresponds to a favor- and CP-conserving interaction which is sensitive to and potentially enhanced by chirality flips. Many high-energy collider observables are insensitive to chirality flips. Many other low-energy observables are chirality-flipping but flavor-violating (b- or K-decays, μ→e conversion, etc) or CP-violating (electric dipole moments). If charged lepton-flavor violation exists, observables such as μ→e conversion can only determine a combination of the strength of lepton-flavor violation and the mass scale of NP.

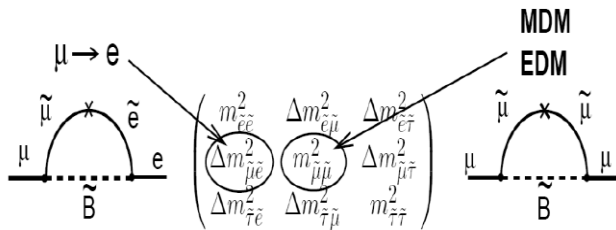
Figure 1.1.1.: The supersymmetric contributions to the anomaly, and to μ→e conversion, showing the relevant slepton mixing matrix elements. The MDM and EDM give the real and imaginary parts of the matrix element, respectively. The × indicates a chirality flip.

In that case, g-2 can help to disentangle the nature of the NP. This implies that a more precise α_μ-measurement will have significant impact on such models and can even be used to measure model parameters. Supersymmetric models are the most well-known examples, so muon g-2 would have substantial sensitivity to the supersymmetric particles. Compared to generic perturbative models, supersymmetry provides an enhancement to $\alpha_\mu(SUSY)$ by a factor tanβ (the ratio of the vacuum expectation values of the two Higgs fields). The SUSY diagrams for the magnetic dipole moment, the electric dipole moment, and the lepton-number violating conversion process $\mu \rightarrow e$ in the field of a nucleus are shown pictorially in Fig. 1.1.1

1.2 Status of the Muon g-2 and Mu2e experiments

The Fermilab E989 experiment (Muon g-2) is on schedule to release its first result (with the BNL E821 statistics) of the measurement of the anomalous magnetic moment of the muon in 2018. The modification of Fermilab accelerator complex will be done by Spring 2017 when the commissioning of the storage ring will start. By that time the various detector subsystems will be installed with the ring inside the experimental hall. The passive shimming of the magnet to produce a highly uniform magnetic field is currently well underway and should complete in the following months, leaving the floor open for the active shimming to start. The final result anticipated for 2020 aims to reduce the total uncertainty of the BNL E821 experiment by a factor four.

The Mu2e experiment design and construction proceeds well and is on schedule to be commissioned with a beam by the end of 2020. The Mu2e experiment has received full CD-3 approval and is preparing to enter full scale production. The detector hall and beamline construction is well under way. Its goal is to probe CLFV with a single event sensitivity of 2.9×10^{-17} or set an upper limit on the conversion rate $< 6 \times 10^{-17}$ at 90 % C.L., thus improving the previous sensitivity by four orders of magnitude. For the long term future (> 2025) the possibility of a Mu2e phase-2 is being explored with the goal of increasing the sensitivity by an additional factor of 10. This can be obtained with a higher beam intensity and a detector capable of handling the the accidental activity occuring from muon capture.

2. Muon g-2 Experiment

2.1 Goal of the Muon g-2 project

It was proposed to measure the muon anomalous magnetic moment, a_μ, to 0.14 ppm - a fourfold improvement over the 0.54 ppm precision obtained in the Brookhaven E821[5] experiment. The muon anomaly is a fundamental quantity and its precise determination will have lasting value. The current measurement was statistics limited, suggesting that greater precision can be obtained in a higher-rate, next-generation experiment. We outline a plan to use the unique Fermilab complex of proton accelerators and rings to produce high-intensity bunches of muons, which will be directed into the relocated BNL muon storage ring. The goal of the experiment is a precision on the muon anomaly of 16×10^{-11}, which will require 21 times the statistics of the BNL measurement, as well a factor of 3 reduction in the overall systematic error.

The measurement of the muon anomaly has steadily improved over more than five decades, with increased experimental precision being matched by commensurate advances in theory. Figure 2.1.1 shows the evolution in the reduction of uncertainty, along with the new goal for the proposed Fermilab experiment. The current experimental uncertainty, determined by Brookhaven E821, has an uncertainty of 63×10^{-11} (0.54 ppm), which is dominated by the statistical error (0.46 ppm). This suggests that a further increase in precision is possible if a higher integrated number of stored muons can be obtained.

It is anchored by the re-use of the existing precision muon storage ring, an efficient and parasitic use of the Fermilab proton complex. During the same time period required to mount, run and analyze the New g-2 Experiment, a vigorous worldwide effort to reduce the uncertainty on the SM contributions will continue.

A new measurement of the anomalous magnetic moment of the positive muon a_μ is also proposed with a novel technique utilizing an ultra-cold muon beam accelerated to 300 MeV/c and a 66 cm-diameter muon storage ring without focusing-electric field at J-PARC[6]. The proposed experiment aims to achieve the statistical errors down to 0.1 ppm like in Fermilab Muon g-2 experiment.
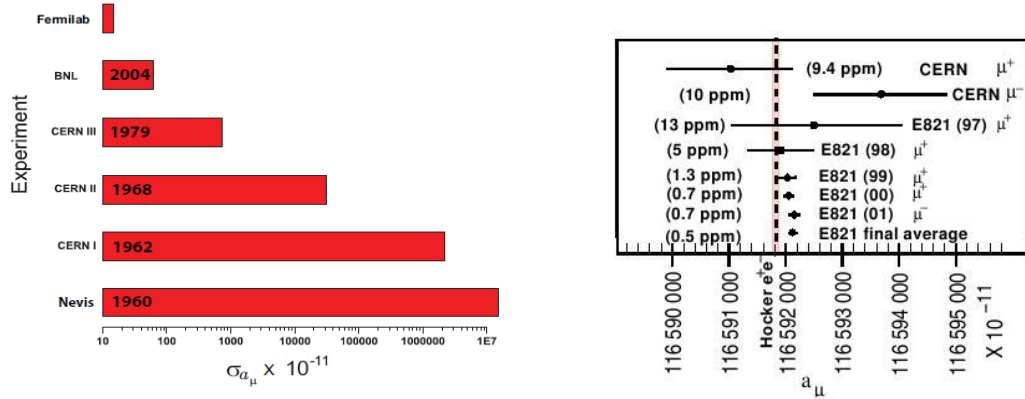

Fig. 2.1.1: a) Graphical display of the achieved uncertainties in the measurement of the muon anomaly, beginning with the Nevis lab experiment in 1960. The goal of our Fermilab experiment improves on the Brookhaven result by a factor of 4. b) History of the precision of the measurements of a_μ at CERN and BNL, compared with the SM prediction.

2.2 Experimental technique

The experiment will be performed by injecting polarized muons into the storage ring, relocated from BNL to Fermilab, and observing the spin precession. The directly measured quantities are the anomalous precession frequency ω_a - the difference frequency between the spin and the cyclotron frequencies - and the magnetic field seen by the muons, which is expressed as the Larmor frequency of a free proton, ω_p. The ratio R of the two leads to the muon anomaly through the relation $a_\mu = R/(\lambda - R)$, where , $\lambda = \mu_\mu/\mu_p$ is the muon-to-proton magnetic moment ratio, determined from muonium hyperfine level splitting [7].

The new experiment will operate in parallel with the high-energy neutrino operation, using a 30% share of protons from the upgraded 8-GeV, 15-Hz Booster. Four short bunches of 10^{12} protons each will be formed for each injected Booster batch. A 3.1 GeV/c positive pion beam will be directed out of the target and along the 290-m AP2 beamline. Most of the pions will decay along the way and the forward-going (0-degree) highly polarized, muons will be captured in the line.
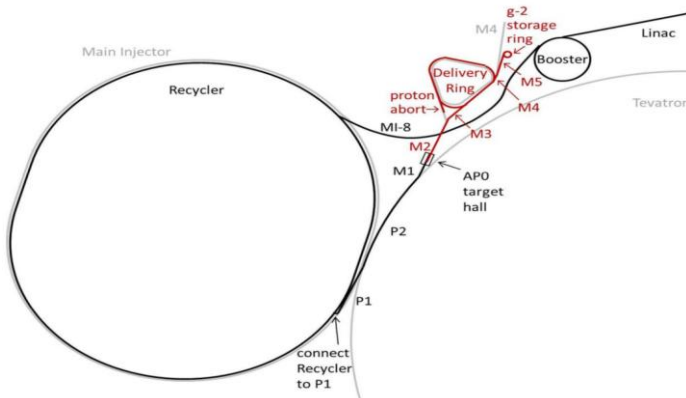

Fig. 2.2.1: Schematic of the Fermilab layout for g-2. A proton batch is delivered from the Booster into the Recycler where it is divided into four smaller bunches by a new rf system. Each bunch is kicked out one-at-a-time and directed to the "antiproton" target at AP0. The pions produced there travel out along the red path toward the Pbar complex and back again to the new MC-1 (Muon Campus one) building, which is located adjacent to the AP0 building.

The decay muons are directed around the antiproton accumulator complex, and then back toward the target region along the parallel transfer line AP3.

The total distance from target to storage ring is approximately 900 m, which allows for efficient muon collection in the forward direction and a sufficient suppression of undecayed pions that enter the storage ring and initiate hadronic showers. The layout is shown in Fig. 2.2.1.

The muon storage ring [8] is a superferric "C"-shaped magnet, 7.112 m in central orbit radius, and open on the inside to permit the decay electrons to curl inward to the detectors (Fig. 2.2.2). A 5 V power supply drives a 5177 A current in the three NbTi/Cu superconducting coils. Feedback to the power supply from the NMR field measurements maintains the field stability to several ppm. The field is designed to be vertical and uniform at a central value of 1.4513 T. Eighty low-current surface correction coils go around the ring on the pole piece faces for active trimming of the field. The opening between the pole faces is 180 mm and the storage region is 90 mm in diameter.
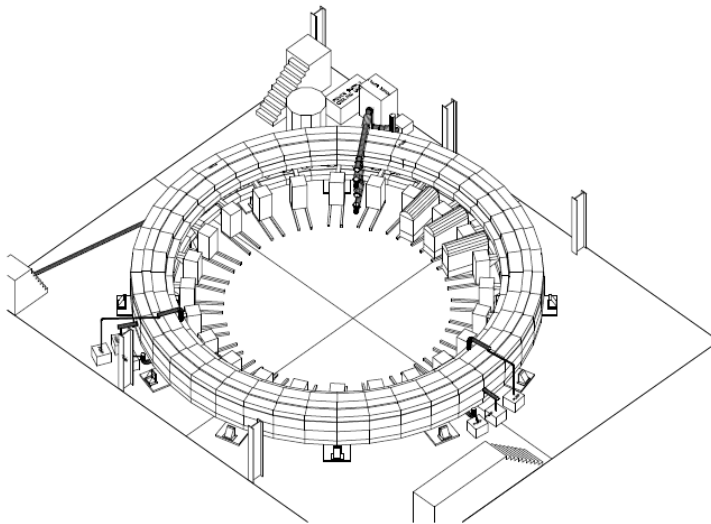

Fig. 2.2.2: A 3D engineering rendition of the E821 muon storage ring. Muons enter the back of the storage ring through a field-free channel at approximately 10 o'clock in the Figure. The three kicker modulators at approximately 2 o'clock provide the short current pulse, which gives the muon bunch a transverse 10 mrad kick. The regularly spaced boxes on rails represent the electron detector systems.

The measurement of ω_a is made by recording the arrival times and energies of decay positrons in a suite of **24 segmented electromagnetic calorimeters**. Coincident events, which penetrate two or three adjacent calorimeter stations, serve as "lost muon" detectors. At three locations around the ring suites of straw chambers, placed upstream of the calorimeters and inside the vacuum chambers, provide detailed beam dynamic information and serve as the basis for a parasitic electric dipole moment measurement.

The detectors, electronics and DAQ, are designed to accept sustained rates per fill up to 3 times as high as BNL E821. The rate comparison is important because it guides upgraded or new systems. First, the instantaneous rate near fit start time determines the pileup fraction, which is a critical systematic uncertainty. Second, the total data flow determines the details of the electronics and DAQ systems, their data transfer rates and the total data storage required. Higher data rates lead to the conclusion that segmented electromagnetic calorimeters are required to reduce the pileup fraction per channel.
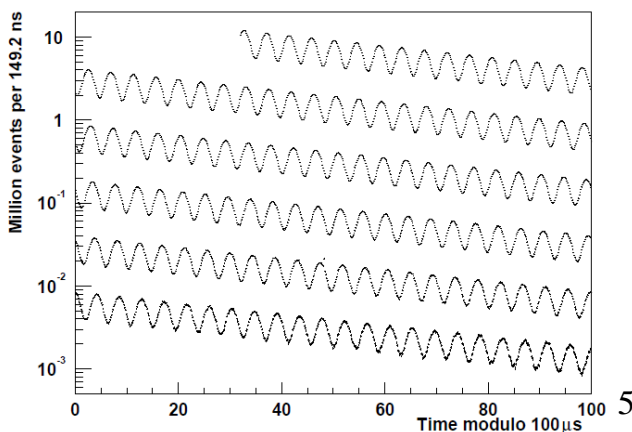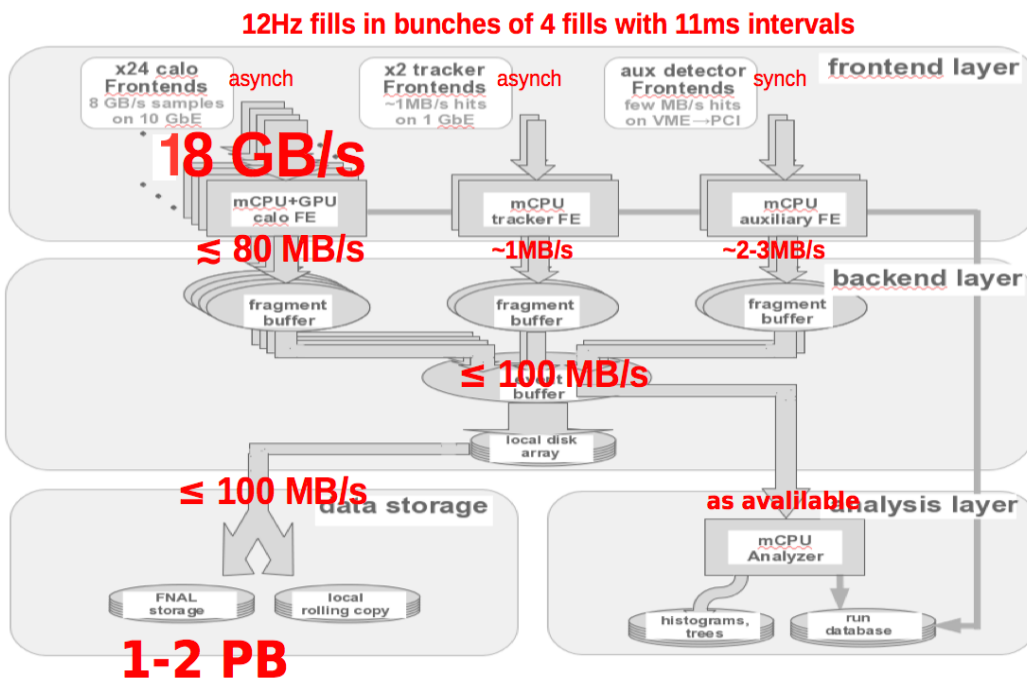

Fig. 2.2.3: Distribution of electron counts versus time for the 3.6 billion muon decays. The data are wrapped around modulo 100 µs.

Positron decays are recorded individually and are sorted by energy and time. For each positron recorded at time t and having energy greater than E_{th}, a single count is incremented in a histogram, such as the one shown in Fig. 2.2.3. The asymmetry A is determined by the choice of threshold, and the statistical power is proportional to NA^2, where N -number of decay electrons per unit energy. Optimizing this figure-of-merit implies setting E_{th} between 1.8 and 1.9 GeV.

DAQ

The detector data acquisition system will provide continuous readout, event building and data storage of the 12-bit, 800 MSPS digitizers instrumenting the 24x54 calorimeter segments, straw tracker and auxiliary detectors. Onboard memories in the digitizers will buffer the raw data and allow its asynchronous readout over 10 Gbit ethernet, thus decoupling the DAQ event cycles from storage ring fill cycles. The frontend layer includes 12 multicore-CPUs with 24 Nvidia Tesla K40 GPUs (288 GB/s bandwidth, 2880 CUDA cores per one GPU) for the calorimeter, one tracker frontend and one frontend for the auxiliary detectors. The frontends will process the digitized records of individual fills into several derived datasets, while a backend layer of multicore CPUs will handle the assembly and storage of the event fragments from the frontend layer. Each stored event will represent a complete record of the activity in the detector systems for each storage ring fill. The DAQ is implemented as a modular, distributed system on a parallel, layered array of networked, commodity PC's running Scientific Linux (SL). The DAQ software is based on the MIDAS data acquisition framework and the ROOT data analysis framework. Data quality monitoring (DQM) software (online analysis layer) will be continuously converting a partial sample of the MIDAS data on-the-fly to ART format, which is standardly used in FNAL for offline data processing and simulation. The online ART data will be processed by a DQM server and the resulting histograms will be accessible via a web interface. So the same ART based programs could be used both for offline and online analysis. The design will also offer the flexibility to construct the T, Q and other datasets at the software level in the frontend CPU/GPU layer. The T-method data will be constructed by saving individual "islands" of above-threshold calorimeter signals and the Q-method data will be constructed by accumulating histograms of fully-digitized fills. This scheme will reduce the 20 GByte/s rate of continuous digitization by a factor of 100. The size of the full data on tape after 2 years of running will be about 2 PB.A separate MIDAS based field DAQ system not tied to muon fills will perform both continuous B-field measurements at fixed points and record data from trolly runs. A custom JavaScript for online data display and MIDAS history for simple trend plot display will be used.

Fig. 2.2.8 Data flow in the g-2 experiment

3. Mu2e Experiment

3.1 Charged Lepton Flavor Violation

Globally there is a very active program searching for CLFV processes using rare decays of muons, taus, kaons, and *B*-hadrons. The ratio of rates among various CLFV processes is model dependent and varies widely depending on the underlying physics responsible. Thus, it is important to pursue experiments sensitive to different processes in order to elucidate the mechanism responsible for LFV effects. The most stringent limits come from the muon sector because of the relative "ease" with which an intense source of muons can be produced. Three rare muon processes stand out, $\mu^+ \rightarrow e^+\gamma$, $\mu^+ \rightarrow e^+e^-e^+$ and $\mu^-N \rightarrow e^-N$. Searches for these processes have yielded null results and set upper limits on the corresponding decay rates. At the 90% confidence level the branching ratio for $\mu^+ \rightarrow e^+\gamma$ must be less than 1.2×10^{-11} [9], the branching ratio for $\mu^+ \rightarrow e^+e^-e^+$ must be less than 1.0×10^{-12} [10], and $R_{\mu e}$(Ti) ($\mu \rightarrow$e conversion on titanium) must be less than 6.1×10^{-13} [11]. In the next decade significant progress on improving these sensitivities is expected only for two of these processes.

The MEG experiment [12] operating at PSI, has a target sensitivity in the range of 10^{-13} – 10^{-14} for the $\mu^+ \rightarrow e^+\gamma$ branching ratio, while the proposed COMET experiment [13] at JPARC and Mu2e at Fermilab would each reach sensitivities of 10^{-16} – 10^{-17} on $R_{\mu e}$(Al). It's important to note that these two decay processes have complementary sensitivity to NP effects and the results from both are helpful in order to untangle the underlying physics. To illustrate this one can estimate the sensitivity of a given CLFV process in a model independent manner by adding lepton-flavor-violating effective operators to the SM Lagrangian,

$$L_{CLFV=\frac{m_\mu}{(1+k)\Lambda^2}\bar{\mu}_R\sigma_{\mu\nu}e_LF^{\mu\nu}+\frac{k}{(1+k)}\bar{\mu}_L\gamma_\mu e_L(\Sigma_{q=u,d}\bar{q}_L\gamma^\mu q_L)}$$

where Λ is the scale of NP and k is an arbitrary parameter controlling the relative contribution of the two terms. If k<<1, the first term, a dimension five magnetic-moment-type operator, is dominant. If k>>1, the second term, a four-fermion interaction-type operator, is dominant. The $\mu^+ \rightarrow e^+\gamma$ process is predominantly sensitive to NP described by the first term, while the $\mu^-N \rightarrow e^-N$ (and $\mu^+ \rightarrow e^+e^-e^+$) process is sensitive to NP described by either term. The NP scale, Λ , to which these two processes are sensitive as a function of k is shown in Figure3.1.1. The projected sensitivity of the MEG experiment will probe Λ values up to 2000 - 4000 TeV for k<<1 scenarios, while having little sensitivity for k>>1 scenarios. The projected sensitivity of the Mu2e experiment will probe Λ values from 3000 to over 10000 TeV over *all* values of k. It should be noted that these effective operators provide a good description of most the NP scenarios in which large CLFV effects might appear in $\mu^+ \rightarrow e^+\gamma^+$ and $\mu^-N \rightarrow e^-N$ decays and the conclusions regarding relative sensitivity are generically true. As demonstrated by Figure 3.1.1, a Mu2e experiment sensitive to rates in the range of 10^{-16} – 10^{-17} is interesting and important in all MEG scenarios.

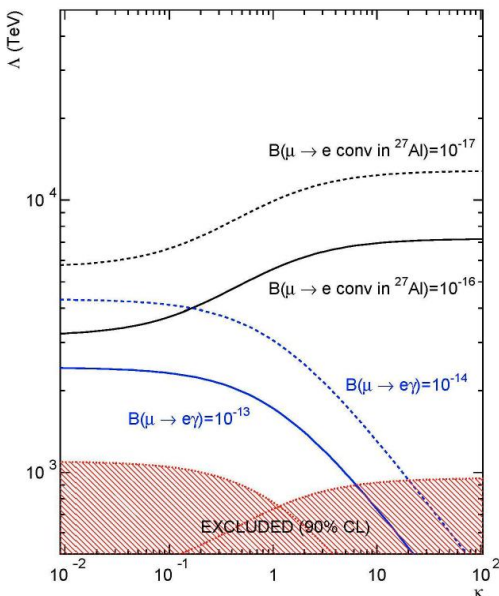Fig. 3.1.1 The sensitivity to the scale of NP, Λ, as a function of k, for a muon-to-electron conversion experiment with a sensitivity of 10^{-16} – 10^{-17} is compared to that for a muon–to-electron-gamma experiment with a sensitivity of 10^{-12} – 10^{-13}. See the text for a definition of k. The excluded region of parameter space, based on current experimental limits, is shaded.

3.2 Signal and Backgrounds for muon conversion experiments

The conversion of a muon to an electron in the field of a nucleus occurs coherently, resulting in a monoenergetic electron near the muon rest energy that recoils off of the nucleus in a two-body interaction. This distinctive signature has several experimental advantages including the absence of accidental backgrounds and the fact that background from muon decay electrons are strongly suppressed near the conversion energy.

When a negatively charged muon is stopped in a target it rapidly ($\sim 10^{-16}$ s) cascades down to the 1S state. Capture, decay or conversion of the muon takes place with a mean lifetime that has been measured in various materials and ranges from ~100 ns to over 2 μs [14]. Neutrinoless conversion of a muon into an electron will produce an electron with an energy that is slightly less that the rest mass of the muon and that depends on the target nucleus:

$$E_e = m_\mu c^2 - B_\mu(Z) - C(A),$$

where Z and A are the number of protons and nucleons in the nucleus, B_μ is the atomic binding energy of the muon and C(A) is the nuclear recoil energy. In the case of muonic aluminum the energy of the conversion electron is 104.97 MeV and the muon lifetime is 864 ns [14]. An electron of this energy, detected in a search window delayed with respect to the muon stop, signals the conversion.

At the proposed Mu2e sensitivity there are potential background processes that can mimic a muon-to-electron conversion signal. Controlling these backgrounds drives the overall design of Mu2e. These backgrounds result principally from four sources: intrinsic processes that scale with the number of stopped muons and includes muon decay in orbit (DIO) and radiative muon capture (RMC), prompt processes where the detected electron is nearly coincident in time with a beam particle arriving at the stopping target, electrons that are induced by cosmic rays, and mis-reconstructed events that result from additional activity from conventional processes that can add tails to the momentum resolution function.

While a free muon decaying at rest can produce an electron whose energy is at most half of the muon rest mass, the decay of a bound muon can result in an electron with energy approaching that of a conversion electron. At the kinematic limit of the bound decay, the two neutrinos carry away no momentum and the electron recoils against the nucleus, simulating the two-body final state of muon-to-electron conversion. The differential energy spectrum of electrons from muon decay in orbit falls rapidly near the endpoint, proportional to $(E_{endpoint}-E_e)^5$. The nuclear recoil slightly distorts the Michel peak and gives rise to a small recoil tail that extends out to the conversion energy.

Radiative muon capture is an intrinsic source of high energy photons that can convert to an electron-positron pair in the stopping target or other surrounding material

Most low-energy muon beams have large pion contaminations. Pions may produce background when stopping in the target or surrounding material through radiative pion capture (RPC) which takes place with a probability of ~ 10^{-2}. The RPC photon spectrum extends beyond the energy of electrons produced by muon-to-electron conversion, so electrons that result from photon conversions in material can produce background. Since pionic atoms decay promptly through the strong interaction, RPC background can be suppressed with the help of a veto counter in the beam, by using a pulsed proton beam or by suppressing the number of pions in the muon beam.

Cosmic rays (electrons, muons, photons) are a copious source of electrons with energies near 100 MeV. If such electrons have trajectories that appear to originate in the stopping target they can fake a muon conversion. With the exception of a cosmic ray photon that produces an electron by converting in the stopping target or other nearby material, these events can be rejected by identifying the incoming particle. Passive shielding and veto counters around the spectrometer help to suppress this background that scales with the experiment's live time rather than with beam intensity.

Low energy electrons combined with random accidental activity in the detector can reconstruct to fake conversion electrons. Additional activity in the detector can originate from the muon beam, from multiple DIO electrons within a narrow time window, and from muon capture on a target nucleus that results in the emission of photons, neutrons and protons. While the rate of accidental background scales with beam intensity, the level ultimately depends on the details of the detector design and the reconstruction software[15,16].

TABLE 3.2.1. Summary of background and error estimates.

Category	Background process	Estimated yield (events)
Intrinsic	Muon decay-in-orbit (DIO)	0.199 ± 0.092
	Muon capture (RMC)	$0.000 \, ^{+0.004}_{-0.000}$
Late Arriving	Pion capture (RPC)	0.023 ± 0.006
	Muon decay-in-flight (μ-DIF)	<0.003
	Pion decay-in-flight (π-DIF)	$0.001 \pm {<}0.001$
	Beam electrons	0.003 ± 0.001
Miscellaneous	Antiproton induced	0.047 ± 0.024
	Cosmic ray induced	0.082 ± 0.018
	Total	0.36 ± 0.10

3.3   Overview of Mu2e

The proposed Mu2e apparatus [15,16] is shown in Figure 3.3.1. An integrated array of superconducting solenoids form a graded magnetic system that includes the *Production Solenoid*, the *Transport Solenoid* and the *Detector Solenoid*. The Production Solenoid contains the *production target* that intercepts an 8 GeV, high intensity, pulsed proton beam. The S-shaped Transport Solenoid transports low energy μ^- from the Production Solenoid to the Detector Solenoid, allows sufficient path length for nearly all of the pions to decay to muons and attenuates nearly all high energy negatively charged particles, positively charged particles and line-of-sight neutral particles. The Detector Solenoid provides a graded field for the stopping target and a uniform field for the *tracker* and the *calorimeter*. The tracking detector is made from low mass straw tubes oriented transverse to the solenoid axis and the calorimeter consists of lead tungstate crystals arranged in four vanes. The electron energy resolution from simulations is ~ 900 keV (FWHM) and is dominated by fluctuations in the energy lost in the target, proton absorber and from multiple scattering in the tracker.

To increase the sensitivity to muon-to-electron conversion by a factor of 10,000 the muon beam intensity for Mu2e will be increased to 10^{11} Hz. This significant increase in intensity is achieved by placing the production target into a graded solenoidal field that varies from 2.5 - 5.0 T, similar to a strategy investigated for the muon collider. A proton beam enters the production solenoid moving in the direction of increasing field strength, opposite the outgoing muon beam direction and away from the detectors. Pions and decay muons moving in the forward direction but outside the loss cone for the field gradient (~30°) will be reflected back by the higher field and will join the backward produced pions following helical trajectories. A large fraction of the confined pions decay, producing muons that accelerate out of the low field region and into another solenoid that transports them to the stopping target. The resulting efficiency is ~0.0025 stopped muons per incident proton.

At the rates required for Mu2e, beam counters can no longer operate efficiently to identify prompt backgrounds. To eliminate prompt backgrounds the Mu2e proton beam will be pulsed. By taking advantage of the relatively long lifetime of the muon in the stopping target it is possible to search for conversion electrons between proton pulses during times when the flux of particles in the secondary muon beam is relatively low. The Fermilab accelerator complex will provide narrow

pulses of protons, separated by about twice the muon lifetime in aluminum, with little or no beam between pulses. The beam structure and the delayed search window are shown in Figure 3.3.2.
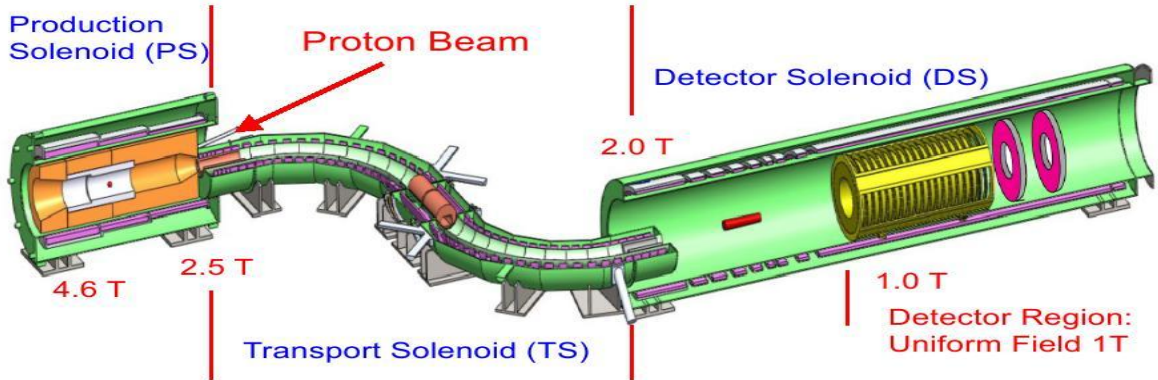

Fig. 3.3.1: The proposed Mu2e apparatus. The Cosmic Ray Veto that surrounds the detector Solenoid and absorbers inside the Detector Solenoid are not shown.

The muon stopping target will be located in a graded solenoidal field that varies smoothly from 2.0 to 1.0 Tesla. The active detector will be displaced downstream of the stopping target in a uniform field region. This configuration increases the acceptance for conversion electrons, suppresses backgrounds and allows for a reduction of rates in the active detector.

Conversion electrons are produced isotropically in the stopping target. Electrons that emerge from the target in the direction opposite the tracking detector (upstream) see an increasing field that reflects them back towards the detector where they can be observed. This essentially doubles the acceptance for conversion electrons. Conversion electrons emitted at $90° \pm 30°$ with respect to the solenoid axis ($p_t > 90$ MeV/c) are projected forward in helical trajectories with large radii that intercept the tracking detector. Beam particles and decay electrons with smaller p_t, representing the vast majority of the rate, pass undisturbed through the evacuated center of the detector. In addition to nearly doubling the acceptance for conversion electrons, the graded field helps to reject background by shifting the transverse momentum of electrons passing through it. Conversion electrons within the acceptance of the detector originate from the stopping target with transverse momenta > 90 MeV/c. The graded magnetic field shifts the transverse momentum of the conversion electrons that reach the tracker into the range between 75 MeV/c $< p_t < 86$ MeV/c. Electrons with a total momentum of 105 MeV/c that are generated upstream of the stopping target cannot reach the tracking detector with more than 75 MeV/c of transverse momentum because of the effect of the graded field, eliminating many potential sources of background.

The active detector is displaced downstream of the stopping target, reducing the acceptance for neutrons and photons emitted from the stopping target and allowing space for absorbers to attenuate protons from the stopping target. This helps to reduce accidental backgrounds. The active detector consists of low mass straw tubes oriented transverse to the Detector Solenoid, a calorimeter constructed from crystals arranged in 2 disks and a cosmic ray veto that surrounds the Detector Solenoid.
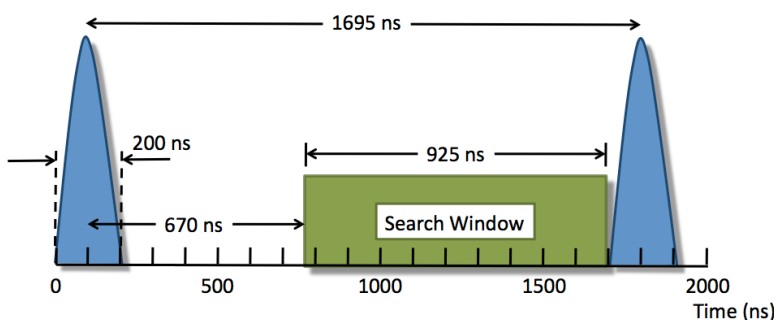

Fig. 3.3.2 The Mu2e spill cycle for the proton beam and the delayed search window that allows for the effective elimination of prompt backgrounds when the number of protons between pulses is suppressed to the required level.

3.4 Mu2e Cosmic Ray Veto.

One major background source for Mu2e is related to cosmic ray muons producing false conversion signal's when interacting with the detector materials. Cosmic-ray muons striking the muon stopping target and other materials in the detector region can produce delta rays that will occasionally be of the right energy and fall within the detector acceptance, producing conversion-like background events. Cosmic ray muons can also decay, producing electrons that could be mistaken for a conversion signal.

The CRV surrounds the Detector Solenoid on 3 sides and extends up to the midpoint of the Transport Solenoid. Comprised of four staggered layers of scintillation counters , the CRV utilizes two embedded Wavelength Shifting Fibers, each readout by means of 2×2 mm^2 Hamamatsu SIPM.

To reduce the background from cosmic rays to 0.05 events over the live time of the experiment the Cosmic Ray Veto must be essentially 100% hermetic on the top and sides. In the region of the muon stopping target the cosmic ray veto must be 99.99% efficient.

The Cosmic Ray Veto must survive an intense neutron flux coming primarily from the muon stopping target. Most of the neutrons have kinetic energies below 10 MeV, with the most probable energy about 1 MeV. Polystyrene scintillator (C8H8) is sensitive to neutrons that elastically scatter on the hydrogen protons, although quenching (Birk's Rule) reduces the light output by an order of magnitude. Studies show that the rate in the counters comes primarily from gammas that are produced from neutron capture on hydrogen. Passive shielding outside the Transport and Detector Solenoids will moderate and capture most of the neutrons. The magnitude and pattern of energy deposition in multiple layers of scintillator is expected to be different for neutrons and muons, which can further help to eliminate false veto signals from neutrons.

The scintillation counters are grouped into modules, with each module having four layers of counters. There are 82 modules, of seven different sizes. Full-size modules contain 64 total scintillation counters, 16 per layer, and are 0.859 m wide, whereas narrow modules have half that number of counters, and are 0.443 m wide. Besides these two different widths, the only difference between modules are their lengths, which range from 0.9 m to 6.6 m. Module masses range from 128 kg to 939 kg. The modules are deployed into six geographical sectors: the upstream (CRV-U) and downstream (CRV-D) regions, the right (CRV-R) and left (CRV-L) sides, and the top sector (CRV-T) (see Fig. 3.4.2).
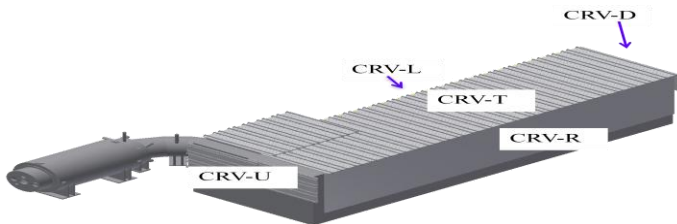

Figure 3.4.2. The cosmic ray veto covering the Detector Solenoid looking downstream, showing the upstream (CRV-U), right (CRV-R), and top (CRV-T) sectors.

3.5   Electromagnetic Calorimeter

The electromagnetic calorimeter is used to form the experimental trigger, to provide a reference time of about 1 ns and space point resolution of about 1 cm for track reconstruction, and a redundant measurement of the electron energy. The calorimeter must operate in a high-rate environment with a radiation dose of about 200 Gy/year. Its response must be suffciently fast that when the detector is turned on 700 ns after the start of the prompt flash, little residual light remains. The calorimeter must be able to operate with no untoward effects in the 1T magnetic field of the detector solenoid. It should have little acceptance for the enormous rate of decay-in-orbit elecions coming from the stopping target, and large acceptance for ~100MeV electrons coming from the stopping target. Its energy resolution must be good enough to enable the trigger to operate at a rate of $\leq$1 kHz.
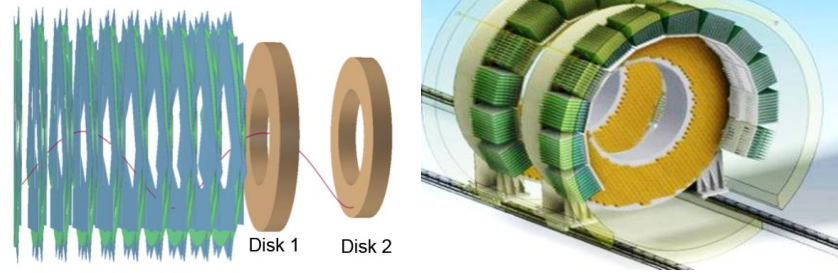
Fig. 3.5.1: a) 3D view of the Mu2e detector showing the straw tracker and the electromagnetic calorimeter, along with the track of a conversion electron. b) CAD drawings of the calorimeter disks. Calorimeter innermost (outermost) radius is of 351 mm (670 mm) with a crystal length of 200 mm. Layout of the FEE and digitization crates is also shown.

The electromagnetic calorimeter system is composed by two disks of scintillating crystals and is placed downstream of the tracker. Similarly to the tracker, the inner circular hole allows to be insensitive to the DIO electrons up to 55 MeV/c momenta. The calorimeter tasks are that of providing a powerful particle identification between muons and electrons, an independent trigger system and a seed for tracking in a complicated reconstruction environment. In order to fulfill these requirements the calorimeter must provide an energy resolution of O(5%), a time resolution < 500 ps and a position resolution better than 1 cm for 100 MeV electrons. The selected crystals should survive a dose of 100 krad and a fluence of up to 10^{12} n/cm^2. The photosensors are shielded by the crystals themselves and should only sustain a fluence of up to 3×10^{11} n_{1MeV}/cm^2.

In the 100 MeV energy regime, a total absorption calorimeter employing a homogeneous continuous medium can meet the resolution requirement. This could be either a liquid such as xenon, or a scintillating crystal; we have chosen the latter. Three types of crystals have been considered in detail for the Mu2e calorimeter: lutetium-yttrium oxyorthosilicate (LYSO), barium fluoride (BaF2) and un-doped Cesium Iodine (CsI). The final selected design for the Mu2e calorimeter uses an array of CsI crystals arranged in two annular disks, as shown in Fig.3.5.1.. Electrons following helical trajectories spiral into the front faces of the crystals, as shown in Fig.3.5.1.right. The crystals are of parallelepiped shape, with a transversal dimension of 34x34 mm^2 and a length of 200 mm; there are a total of 1348 crystals. Each crystal is read out by two large-area silicon photomultipliers (SiPM); solid-state photo-detectors are required because the calorimeter resides in a 1 T magnetic field. Front-end electronics is mounted on the rear of each disk, while voltage distribution, slow controls and digitizer electronics are mounted in crates located on top of each disk. A laser flasher system provides light to each crystal for relative calibration and monitoring purposes. A circulating liquid radioactive source system provides absolute calibration and an energy scale. The crystals are supported by a lightweight carbon fiber support structure in the inner region and by an aluminum support in the outer region.

4. **JINR CONTRIBUTION**

The aim of the current PROJECT is to continue the process for JINR to participate in the Muon g-2 and Mu2e experiments. This includes R&D and design activities, simulations, data acquisition, data taking and data analysis. JINR physicists stationed at Fermilab would play a role in the integration, installation and commissioning of the Muon g-2 and Mu2e detectors.

This Project is carried out in the framework of the MoU between FERMILAB and JINR concerning scientific cooperation in Muon g-2 and Mu2e experiments in particular and "Statement of work for participation in the Mu2e Experiment at Fermilab between Fermi Research Alliance, LLC, Illinois (USA) and The Joint Institute of Nuclear Research". The present PROJECT will cover the activities and commitments detailed bellow.

The detailed description of the contribution of JINR scientists in experiments over the past 3 years and plans for the future is given in the full text of the Project, see also ref. [d1-d18,c1-c8]. Here we present the cumulative Tables of working status and plans of JINR group and planned expenses for 3 years.

The full time equivalent (FTE) in this Project is about 19 persons from JINR side.

Working status and plan (summary)   Muon g-2 experiment

Done	In progress	New
Online data quality monitoring (DQM) software for the calorimeter prototype using the ROME (Root based Object oriented Midas Extension) framework has been developed and successfully used during test run at SLAC in April 2016. **Prototype of the straw tracker** with 1 mm longitudinal space resolution was created and tested successfully.	**A development of an online event display program** based on PARAVIEW data analysis and visualization software is in progress. The real time data from the detector will be transferred to a special server where the MIDAS data are converted on-the-fly to the ART format.(2018-2019) **MIDAS online alarm system development and support**. Integration of all required alarms from different experiment subsystems into the central MIDAS DAQ. Testing and debugging of the new alarm system during engineering runs before data taking. Support of the alarm system during beam runs. (2018-2020)	**MIDAS ODB support and interfacing** Development of new custom JavaScript web pages for the MIDAS ODB control. Special applications scripts for checking ODB integrity and correcting possible errors. (2018-2020) **Participation in the test and data taking runs** Participation in final integration and testing of the full DAQ system .Expert support of the MIDAS software during physical runs 2018-2020. **Analysis of the physical data** (2018 ->)

Working status and plan (summary)   Mu2e experiment (calorimeter)

Done	In progress	New
E.m. calorimeter simulation LYSO, CsI crystals and matrix simulation: time, energy resolution, longitudinal uniformity **prototype Lyso crystal matrix (3x3) tests** at electron beams at Frascati and MAMI, and data analysis **prototype CsI crystal matrix (3x3) tests** (with PMT) at Yerevan electron accelerator (15-35 MeV) and data analysis **prototype CsI crystal matrix (3x3) tests** (with SiPM) at	**E.m. calorimeter simulation** Calorimeter in situ calibration methods (2018-2020) **Preparation to the crystal tests at JINR electron accelerator LINAC-800.** Testing the accelerator in the low intensity operation and background conditions. (2018-2020) **RnD with BaF$_2$ crystals and solar blind photodetectors.** (2018-2020)	**CsI crystals QA tests** at Yerevan electron accelerator (15-40 MeV e$^-$ beam) and data analysis (2018-2020) **CsI crystals QA tests at Frascati electron accelerator** (70-120 MeV) (2018-2020) **CsI crystals QA tests at DLNP lab** on radioactive sources and cosmic muons (2018-2020) **Participation in the calorimeter assemble and commissioning** (2020) **Participation in the data**

		analysis (2021 ->)
Frascati electron accelerator (70-105 MeV) and data analysis **Radioactive sources test of CsI crystals at DLNP lab.** Longitudinal response uniformity and ratio fast to total scintillation component		

Working status and plan (summary)   Mu2e experiment (CRV)

Done	In progress	New
Simulation of the CRV counters characteristics under different test conditions and optical resin filling **Increasing the light yield from scintillation strips .** The method of parallel filling of several fiber channels is developed. The measured light yield of the strip filled with optical resin SKTN-MED(E) in average is 1.5-1,8 times higher than that of the "dry" strip **Test beam of the CRV counter prototypes.** Participation in the tests at 120 GeV proton beam and data analysis **Technology of the CRV 4-layers module assembly is developed and pilot module is produced**	**Simulation of the CRV efficiency** in the experimental setup (2018-2019) **Radiation hardness tests of the scintillator strips and filler samples at the JINR IBR-2 facility are performing** (2018)	**Test beams of the SKTN filled counters** (2018) **Design and creation of the stand for QA testing** of the produced CRV 4-layers modules up to 6.6 m length (2018) **Control on the CRV modules production and QA tests** of the manufactures CRV modules (2018-2020) **Participation in the CRV system assemble and commissioning** (2020) **Participation in the data analysis (2021 ->)**

plan of expenses for materials and travel

#	Activity	support	Resources (k$)		
			2018	**2019**	**2020**
	Muon g-2				
	DAQ computers	Apple Mac Pro, servers	5	5	5
	Hardware for DAQ development	Micro TCA crate and units	20	20	20
	DAQ start up, maintenance, data taking shifts (phys. Runs from 2018)	scientific trips	25	25	25

	Mu2e				
	Calorimeter in-kind contribution	200 CsI crystals (34x34x200 mm^3)	100	100	100
	Upgrade DLNP rad sources and cosmic muons test stands	NIM logic units, VME flash ADC, power supplies, coordinate table, SiPM's , preamplifiers, scopes	40	30	20
	Development of the JINR Linac-800 crystal test stand	coordinate table, power supplies for trigger counters, NIM and VME units	20	10	
	Crystals beam and QA tests at Frascati, Fermilab and Yerevan, front end electronic development and calorimeter construction, tests, simulation	scientific trips to Frascati, Fermilab, Yerevan	28	28	26
	R&D on BaF2 photodetectors	AlxGa(1-x)N photocathodes and avalanche photodiode, BaF2 crystal samples	10	10	20
	Tests of the CRV counters at Fermilab beam	scientific trips to Fermilab	12	12	14
	Development of the CRV modules assemble procedure and creation of the QA stand for tests of the produced modules	scientific trips to Virginia University	20	20	20
	Computers and accessories		5	5	5

The presented above expensive plans are reasonable and rather detailed. The standard Project Forms 26, 29 are signed and delivered to the JINR Science Organization & International Cooperation Office.

5. SWOT analyses

The **strengths** of the Project is its fundamental physical importance in the search for new physics as a project complimentary to the search for new particles and phenomena with modern powerful accelerators. Both experiments are international, approved by the DOE and got full Critical Decision-3 (CD-3) that gives reason to believe that these experiments will be performed. Muon g-2 will have technical run in 2017 and will start to collect data since 2018. Mu2e will implement the creation and assembly of solenoids and detectors in 2018-2020 and will start physics run in 2021.

   Weaknesses is the probability of not finding the new physics that will automatically leads to setting a new limit on the process of converting from the muon to the electron and the parameters of the corresponding models of new physics. There is currently no reliable SiPM's for crystals of the BaF2 calorimeter, planned in the 2-nd phase of the experiment with approximately 2025. The JINR group is actively involved in research in this direction.

   Threats to our group are related to the potential lack of funding which can lead to different consequences. In the event of failure to plan for calorimeter in-kind contribution prescribed in "Statement of work..." will lead to a problematic perception us as a reliable partner and will increase the burden on the budget of the Italian colleagues, who have overall responsibility for the calorimeter. Insufficient funding may also impact on equipping our laboratory in DLNP for quality control crystals and the carrying out of works on assembling and CRV modules QA tests and participating in different test runs that are likely to lead to behind schedule on the creation of the calorimeter and the CRV system.

References

1. R.M. Carey, K.R. Lynch, J.P. Miller et al, "The New (g-2) Experiment: A proposal to measure the muon anomalous magnetic moment to +-0.14 ppm precision", FERMILAB-PROPOSAL-0989, (2009).
2. R. M. Carey, et al. (Mu2e Collaboration), Fermilab Proposal 0973 (2008).
   R.J. Abrams et al., "Mu2e Conceptual Design Report", arXiv:1211.7019 (2012). Mu2e collaboration, "Mu2e Technical Design Report (TDR)", arXiv:1501.05241, Fermilab-TM-2594, Fermilab-DESIGN-2014-01
3. Y. Kuno and Y. Okada, *Rev. Mod. Phys.* 73, 151 (2001) *and* M. Raidal, *et al.*, Eur. Phys. J. C57, 13 (2008).
4. R.M. Djilkibaev and V.M. Lobashev, Sov. J. Nucl. Phys. 49(2), (1989) 384; V.S. Abadjev, et al., INR Preprint 786/92 (1992).
5. G.W. Bennett et al.," Final report of the E821 muon anomalous magnetic moment measurement at BNL", Phys. Rev. D 73, p.072003 (2006).
6. Letter of Intent: An Improved Muon (g − 2) Experiment at J-PARC (2003), New approach to the Muon g–2 and EDM experiment at J–PARC, Journal of Physics Conference Series 295(1):012032 · May 2011
7. W. Liu et al., Phys. Rev. Lett. 82, 711 (1999).
8. G.T. Danby, et al., Nucl. Instr. and Methods Phys. Res. A 457, 151-174 (2001).
9. M. Ahmed, *et al.* (MEGA Collaboration), Phys. Rev. D65, 112002 (2002).
10. U. Bellgardt, *et al.* (SINDRUM Collaboration), Nucl. Phys. B299, 1 (1988).
11. J. Kaulard *et al.*, Phys. Lett. **B422**, 334 (1988).
12. J. Adam, *et al.* (MEG Collaboration), Nucl. Phys. B843, 1 (2010).
13. COMET, Y.G. Cui et al., CDR, KEK-2009-10
14. T. Suzuki *et al.*, Phys. Rev. **C35**, 2212 (1987).
    A. V. Artamonov et al., Phys. Rev. D 79, 092004 (2009).
15. J. R. Abrams et al, Mu2e conceptual design report.
16. L. Bartoszek, et al., Mu2e Technical Design Report arXiv:1501.05241.

Our publications and conference reports connected to this Project

d-1. N.A. Kuchinskiy, V.A. Baranov, V.N. Duginov et al., , 2-D straw detectors with high rate capability // arXiv:1502.05363; *accepted for publication in   Particles and Nuclei, Letters.*
d-2. Kuchinskiy N. A., Baranov V. A.Zyazyulya. et al. , Using the Cathode Surface of Straw Tube for Measuring the Track Coordinates Along the Wire // arXiv:1105.2258.; Instrum.Exp.Tech. 2012, V. 55, 26-28.
d-3. N.A.Kuchinskiy, V.A.Baranov, V.N.Duginov et al., *The use of segmented cathode of a drift tube for designing a track detector with a high rate capability* // JINR preprtin 313-2013-100; arXiv:1310.5065; Instrum.Exp.Tech. 57 (2014) 553-55.
d-4. The muon g-2 experiment at Fermilab - Gohn, W., for the Muon g-2   Collaboration arXiv:1611.04964 [hep-ex] FERMILAB-CONF-16-529-E.
d-5. J. Budagov et al., "The calorimeter project for the Mu2e experiment", Nucl. Instr.&Meth. A718(2013) 56-59.
d-6. O. Sidletskiy et al., "Evaluation of LGSO:Ce scintillator for high energy physics experiments", Nucl. Instr.&Meth. A735(2014) 620-623.
d-7. K. Afanaciev et al., "Response of LYSO:Ce scintillation crystals to low Energy gamma-rays", Part. Nucl. Lett. (2015), Vol. 12 (193), p.476

d-8. Z. Usubov, "Electromagnetic calorimeter simulation for future $\mu \to e$ conversion experiments", arXiv:1212.4322 (2012).

d-9. Z. Usubov, "Light output simulation of LYSO single crystal", arXiv:1305.3010 (2013).

d-10.   N. Atanov et al., "Measurement of time resolution of the Mu2e LYSO calorimeter prototype", Nucl. Inst. Meth. A 812 (2016), 104.

d-11.   N. Atanov et al., "Design and status of the Mu2e electromagnetic Calorimeter", Nucl. Inst. Meth. A 824 (2016), 695.

d-12.   Z.Usubov, "Scintillation light simulation in big-sized BaF_2 and pure CsI crystals" http://arxiv.org/abs/1604.00827

d-13.   N.Atanov et al., "Characterization of a prototype for the electromagnetic calorimeter of the Mu2e experiment" IL NUOVO CIMENTO 39 C (2016) 267

d-14.   N. Atanov et al, "Energy and time resolution of a LYSO matrix prototype for the Mu2e experiment" NIM A824, 11 July 2016, Page 684

d-15.   N. Atanov et al, "Characterization of a 5 × 5 LYSO Matrix Calorimeter Prototype" IEEE TRANSACTIONS ON NUCLEAR SCIENCE, VOL. 63, NO. 2, APRIL 2016, p.596

d-16.   M.Angelucci et al., "Longitudinal uniformity, time performances and irradiation test of pure CsI crystals" Nucl.Instrum.Meth. A824 (2016) 678

d-17.   A. Artikov et al. "Optimization of light yield by injecting an optical filler into co-extruded hole of the plastic scintillation bar." JINST 11 (2016), T05003.

d-18.   A. Simonenko et al., " The increase of the light collection from scintillation   strip   with hole for WLS fiber using various types of fillers" , submitted to Part. Nucl. Lett. (2016), in Russian, arXiv:1604.02286.

Our conference talks

c-1   Baranov V.Y., JINR, "Research of properties undoped crystals CsI" Fifth International Conference ISMART 2016 "Engineering of Scintillation Materials   and   Radiation Technologies" , 26 - 30 September 2016

c-2   Atanov N.V., Ivanov S.V., Jmeric V.N., Nechaev D.V., Tereshchenko V.V. "Solar-blind photodetectors with AlGaN photocathodes for light registration in   UVC range" conference NTIHEP-2016, Montenegro, Budva

c-3   Kharzheev Yu.N., "New trends in using Scintillation counters in modern high energy experiments" THE 6th INTERNATIONAL CONFERENCE ON CONTEMPORARY PHYSICS, June 7-10, 2016, Ulaanbaatar Mongolia

c-4   Vasilyev I.I., JINR, « The light yield of a long scintillation strip with WLS fiber embedded into the co-extruded hole » Fifth International Conference ISMART 2016 "Engineering of Scintillation Materials and Radiation Technologies" , 26 - 30   September 2016

c-5   A.Simonenko et al, «INCREASING THE LIGHT YIELD FOR   SCINTILLATION STRIPS WITH WLS FIBER EMBEDDED INTO THE CO-EXTRUDED HOLE» New Trends in High Energy Physics, 2016, Montenegro,   Budva

c-6   Kharzheev Yu.N., "Scintillation Detectors in modern High Energy Physics Experiments and Prospect of their use in Future Experiments", International Conference on Astrophysics and Particle Physics, December 8-10, 2016, Dallas, USA

c-7   N. V. Khomutov, "Using the cathode surface of straw tube for measuring the track coordinate along the wire and increasing rate capability", New Trends in High-Energy

Physics. Budva, Becici, Montenegro, 02 October - 08 October, 2016.

c-8   N. P. Kravchuk, *"Tracker* prototype on a base of cathode straw*",* Fifth International Conference ISMART 2016 "Engineering of Scintillation Materials and Radiation Technologies", September 26-30, 2016, Minsk, Belarus.

Agreements

1. Memorandum of Understanding Between The Joint Institute for Nuclear Research and Fermi National Accelerator Laboratory Concerning Cooperation in Particle Physics and Related Fields, signed by FNAL and JINR Directorate at April 22 2013 for 5 years. It intends JINR to cooperate in Muon to electron conversion (Mu2e) experiment and Muon g-2 experiment at Fermilab.

2. IMPLEMENTATION AGREEMENT to the Memorandum of Understanding between Dzhelepov Laboratory of Nuclear Problems of the Joint Institute for Nuclear Research and the Mu2e Experiment concerning scientific cooperation signed by Mu2e Spokespersons and JINR DLNP Directorate at December 2013 for 3 years.

3. THE NON-PROPRIETARY USER'S AGREEMENT BETWEEN JOINT INSTITUTE OF NUCLEAR RESEARCH, DUBNA, AND FERMI RESEARCH ALLIANCE, LLC DATED August 18, 2015

4. Statement of work For participation in the Mu2e Experiment at Fermilab between Fermi Research Alliance, LLC, Illinois (USA) and The Joint Institute of Nuclear Research, Dubna, Russia. February 2017.